Submitted to NUCLEAR INSTRUMENTS
AND METHODS

LBL-7995
Preprint

ION IDENTIFICATION BY DETECTOR TELESCOPES

F. S. Goulding

March 1978

Prepared for the U. S. Department of Energy
under Contract W-7405-ENG-48

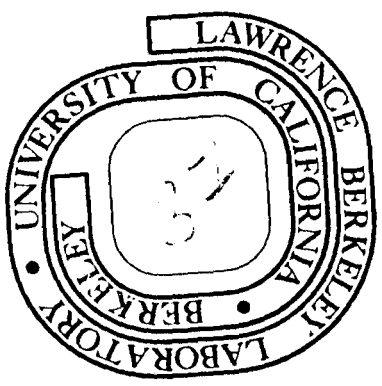

DISCLAIMER

LBL-7995

ION IDENTIFICATION BY DETECTOR TELESCOPES*

F. S. Goulding

Lawrence Berkeley Laboratory
University of California
Berkeley, California 94720 U.S.A.

Abstract

This paper discusses the identification of ions produced in nuclear reactions. The use of detector telescopes to provide energy loss information and the manipulation of the ΔE and E signals to identify the ions is emphasized. The value of combining this method with measurement of mass by time of flight between the detectors, and thereby producing a two-dimensional M v MZ^2 picture is illustrated.

* This work was supported by the Physical Research Division of the Department of Energy under Contract No. W-7405-ENG-48.

Introduction

Reactions between high-velocity nuclear projectiles and target nuclei provide an important probe of nuclear structure. Identification of particles emitted from the target and measurement of their energy are essential parts of this technique. Since heavy highly-charged particles produce denser ionization tracks than light ions of the same energy, it is intuitively obvious that a simultaneous measurement of the energy, range and ionization pattern along a particle's track may suffice to identify the nature of the particle. This type of evidence was used even in the days of the Wilson cloud chamber and has been increasingly employed in the past 20 years as a particle identification technique. Modern detector telescope identifiers used one or more ΔE transmission detectors to sample ionization along the track and an E detector to absorb the remaining energy of the particle. The summed ($\Delta E + E$) signal gives a measure of the total particle energy and the pattern of ΔE and E signals provides identification.

As we will see, unambiguous identification of every isotope is not possible with simple detector telescopes; consequently, other particle-sensitive effects may be used to augment the ionization information. Thus, for example, its time of flight between two well-spaced detectors (e.g., ΔE,ΔE or ΔE,E) can be used to directly determine a particle's velocity. Also, the magnetic rigidity of the particle may be used to measure its momentum to charge ratio. Each type of measurement is sensitive to different combinations of particle parameters and is subject to measurement errors. Consequently, depending on the specific case, one or more of these methods may be required to uniquely determine the mass and atomic number of a particle.

This short paper concentrates on detector telescope identification, including the use of time of flight in addition to the classical simple ionization measurement. For an extensive bibliography readers are referred to Ref. 1. Historically, the first use of modern detector telescope identifiers was reported in 1958[2]), although the use of semiconductor detectors, which has dominated the field for the past 15 years, came somewhat later[3]). While time of flight measurements have been

rather common in very low-energy experiments, the first reported use of combined ΔE,E and time of flight measurements was in 1966[4]). The use of two ΔE detectors for improved performance in studying low-yield reactions was first reported in 1966[5,6]). Multiple detector telescopes for analysis of very high energy particles were first reported in 1972[7]).

Manipulation of ΔE and E signals usually involves using a convenient algorithm to generate a parameter whose value is characteristic of a specific type of ion. Early work used a $\Delta E \cdot E$ "multiplier" algorithm based directly on the Bethe-Bloch equation which describes the rate of energy loss by ionization along a particle's track. This algorithm depends on the energy loss in the ΔE detector being small compared with the total energy and experimental adjustment of two free parameters is also required. Development of a power-law range-energy algorithm in 1964[8]) provided a convenient way to overcome these difficulties. While on-line identification was always performed by analog particle identifiers in early work, the past few years have seen increasing use of digital computers for this function. While computer methods tend to be slower, and analysis is often performed off-line on recorded (event by event) data, they allow the use of more sophisticated identification algorithms. On occasion, on-line analog identification is performed as a coarse filter and the selected events are then subjected to refined computer analysis.

Recognition of light ions, such as protons, deuterons, tritons, ^{3}He and ^{4}He ions is not difficult because the relative change in energy loss between successive isotopes is quite large. Furthermore, except at quite low energies, these ions are fully stripped and their charge is equal to their atomic number Z. As identification of heavier ions is attempted, the problem becomes much more difficult since energy losses of adjacent ions are not very different from each other and, furthermore, the effectively charge in the ions may no longer be equal to Z. The growing interest in heavy ion physics has therefore changed the perspective on particle identification.

Detector Telescopes

Particle identification essentially depends on detectors which provide energy loss information. The simplest type of ΔE,E detector telescope system is shown in Fig. 1 where incident ions pass through the ΔE detector and stop in the E detector. Signals from the detectors are amplified and, if that they meet certain time coincidence and amplitude criteria, are added together to provide a total energy signal. At the same time, they are processed in the identifier to provide a particle-identity signal.

A more complex identifier is shown in Fig. 2. Here two ΔE detectors replace the single one of Fig. 1 and an extra detector, E_{REJ}, at the rear of the E detector, is used to reject all particles that pass through the E detector. This permits total rejection of a high rate of unwanted particles, such as long-range incident ions elastically scattered from the target, which might otherwise produce false identification signals. The use of two ΔE detectors allows two simultaneous identifications to be made on each particle. Comparison of these permits rejection of events where an excessively large or small energy loss occurs in one of the thin ΔE detectors. This type of telescope is particularly useful where a low-yield product must be studied in the presence of many particles produced by more probable reactions. The effectiveness of the technique is illustrated by the identifier output spectra shown in Fig. 3. The triple-detector identifier (ΔE_2, $E\Delta_1$, E) clearly produces much better resolution of the isotope peaks than does the double-detector identifier (ΔE,E). The first use of this method was to prove the stability and to determine the mass of ^{8}He. Figure 4 shows the identifier spectrum obtained in this experiment; the ^{8}He events represent only 1 in 10^9 of the total number of particles passing through the telescope.

These examples, which illustrate the types of results obtained with detector telescope identifiers, employed silicon detectors for both ΔE and E measurements. This choice is not universal. Thus early work used scintillation detectors despite the fact that such detectors are far from ideal in the linearity of their energy response. Early work also used gas ionization detectors for ΔE measurements because of

difficulties in fabricating totally-depleted thin silicon detectors. Recent interest in the physics of short-range heavy ions, has resulted in a resurgence of gas ionization chambers. At the other end of the scale, silicon detectors may be replaced by telescopes of up to 10 or more thick (>1 cm) germanium detectors where very long-range particles are to be identified. For the purpose of this brief paper, we will concentrate on the use of silicon detector telescopes while drawing attention to the application of other detectors where it is appropriate.

Choice of ΔE and E detector thicknesses is dictated by the ranges of the ions to be measured. Figure 5 shows the range of light ions (H and He ions) in silicon. As one example of a detector telescope, we might use the case of identification of ions in the range of 50 MeV α particles. Here the total particle range is approximately 2 mm of silicon, so an E detector 3 mm thick might well be used. The ΔE detector thickness might generally be expected to be a small fraction of the E detector thickness (e.g., 200 μm), but the actual value chosen depends on the minimum range particles to be measured. Clearly, all particles of interest must penetrate into the E detector and produce a reasonable signal there. In this type of experiment, a relatively thick E detector is required. This requirement can be satisfied by lithium-drifted silicon detectors or by surface barrier detectors made on rare, very high resistivity (50 kΩ·cm) silicon. The much thinner ΔE detector requirement can easily be achieved by surface barrier detectors or by diffused or ion-implanted junction detectors. However, it is important to note that all ΔE detectors must be totally depleted and sensitive throughout their thickness. Dead layers on either face must be of negligible thickness for good determination of the particle energy. Dead material is particularly serious between the ΔE and E detectors since it results in the E detector receiving the particles at a different energy from that on leaving the sensitive volume of the ΔE detector. This means that the exit surface on the ΔE detector and the entry surace on the E detector must both represent negligible dead layers. For medium and long-range particles, such as 50 MeV α particles, these requirements are easy to achieve since typical dead layers in

diffused, ion implanted and surface barrier detectors are <0.25 μm. However, this becomes a more serious problem in heavy-ion applications.

The practical upper limit to the thickness of silicon detectors is approximately 5 mm which roughly corresponds to the range of 30 MeV protons. To accommodate longer-range particles, multiple detectors must be used. For example, silicon detector telescopes containing up to ten 5 mm thick detectors are being used in satellite experiments for the isotopic analysis of cosmic rays[9]). This work, which requires the study of isotopes as heavy as those of iron, places very severe demands on the detectors. Lithium-drifted detectors, specially developed for this purpose, are uniform to ±10 μm in their 5 mm thickness over a circular area 5 cm in diameter. Furthermore, the typical 100 μm--thick lithium diffused region on the n^+ face of the detector cannot be tolerated. Therefore, the detectors developed for this type of experiment are treated by removing the normal lithium-diffused region after drifting and performing a relatively low-temperature lithium diffusion to produce a very thin (<10 μm) uniform n^+ surface layer.

Germanium detectors (either high-purity or lithium-drifted) can be produced in thickness as large as 1.5 cm. Furthermore, it is possible to produce telescopes of up to 10 high-purity germanium detectors (in contrast to lithium-drifted detectors where handling is extremely difficult). Therefore, telescopes with a total mass of approximately 80 g/cm^2 can, in principle, be fabricated. One disadvantage of using germanium detectors is that low temperature (~77° K) operation is essential, but this is the only satisfactory approach to analysis of very long-range particles and the technique is rapidly being exploited[10]). Nuclear reactions and small angle scattering in the detectors, which cause loss of particles from the telescope, represent obvious limitations in this technique. However, since many observations are made along the particle track, the pattern of ionization provides the required information to reject particles suffering reactions or serious scattering.

While long-range particles require massive detectors, the reverse is true in the case in low- to medium-energy heavy-ions where much of the interest in particle identification now centers. Figure 6 shows

the ranges of some representative heavy ions in silicon. As an example of a heavy-ion identifier telescope, we consider one suitable for identification of 100 MeV oxygen ions. Since the range of such ions is approximately 200 μm in silicon, a suitable E detector might be 300 μm in thickness. This is a convenient size for surface barrier detectors or for diffused or ion-implanted junction detectors. The required ΔE detector thickness is ~25 μm which can be achieved by similar detector techniques. However, it is obvious that heavier or lower energy ions require thinner ΔE detectors. Several difficulties in fabricating suitable silicon ΔE detectors then become important:

(i) Handling very thin (<10 μm) silicon slices is extremely difficult.

(ii) Producing the required thickness uniformity (say <0.1 μm) presents serious problems.

(iii) The surface dead layers produced by typical diffusion, ion-implanting or surface barrier processes tend to be approximately 0.1 μm in thickness. This thickness is large enough to be objectionable when the total detector thickness is much less than 10 μm.

Despite these problems, special methods such as preferential etching of epitaxially-grown layers of silicon[11]) have been developed which have made possible the fabrication of ΔE detectors a few μm thick.

As interest in the physics of very heavy ions grows, it becomes obvious that silicon detectors, so long the basis for detector telescope identifiers, are no longer the appropriate devices. A 10 μm silicon thickness corresponds approximately to 2.5 mg/cm^2 which, coincidentally, is equivalent to a few centimeters of typical gases at atmospheric pressure. Therefore, it seems natural to use gas ionization ΔE detectors for very heavy ions. The major advantage of semiconductor detectors--the small value of the energy required per hole-electron pair, which results in good statistics and signal/noise ratio--is no longer a real advantage for heavy ions where other processes mainly determine the energy resolution. Furthermore, radiation damage in silicon is a major problem in heavy-ion experiments while it does not

occur in gas detectors. Consequently, recent years have seen increasing use of gas detectors as ΔE detectors (with accompanying silicon E detectors) or, sometimes, as both E and ΔE detectors for very short-range ions.

An example[12]) of a gas ΔE detector used with a silicon E detector is shown in Figs. 7 and 8. The silicon surface barrier detector is mounted in the gas volume at the end of the particle tracks. Particles enter the gas detector through a very thin plastic (20-60 $\mu g/cm^2$) window which serves to contain the continuously flowing counter gas (Ar + 10% CH_4), which is at a pressure of 70 torr. The pressure at the left of the entry window is that of the scattering chamber vacuum so the window must withstand the 70 torr pressure across it. The path length of ions in the gas (~7 cm) corresponds to a thickness <1 mg/cm^2 and a lower gas pressure will reduce this thickness accordingly. Therefore in its normal mode, the gas ΔE detector is roughly equivalent in its energy absorption to a silicon detector less than 4 μm thick. The fact that the electronic charge signal is roughly 10 times smaller than that in the equivalent silicon detector is not a serious problem when measuring heavy ions.

The gas detector is essentially a gridded ion chamber with the anode shielded from movement of charges in the main gas volume by the presence of the grid. The potential distribution shown in Fig. 8 shows that a rather strong focussing action occurs for electrons being collected; this largely eliminates the effects of transverse diffusion of the electrons during collection.

One respect in which gas detectors are much inferior to semiconductor detectors is in their poor timing performance. While this is of little consequence for standard ΔE,E identifiers, it becomes a serious limitation when time of flight measurements are combined with ΔE,E identification. This technique will be discussed later.

Processing ΔE,E Signals

Since complex nuclear reactions produce many types and energies of reaction products, the pattern of ΔE and E signals can be very complex. For example, the case of bombarding copper with argon ions is shown in

Fig. 9. This result was obtained with the gas ΔE, silicon E detector system shown in Fig. 7. In this case, the ΔE,E pattern indicates the presence of at least 27 elements in the reaction products. While Fig. 9 does not provide information on isotopic abundances of these elements, such information is often required and can sometimes be obtained for the lighter fragments.

The processing of such information in a convenient and fast way to allow selection of specific isotopes and then to permit examination of the energy distribution of each of these isotopes has occupied much attention. As a recent extreme example, we might cite the pattern recognition methods applied to data on the type shown in Fig. 9 by Glassel, et.al.[13]). Here, the map shown in Fig. 9 is examined and correlation techniques are used to exploit the systematics evident in the map. Providing that the yield curves for the elements vary smoothly from one element to the next, these methods permit a reasonable determination of the relative yields of elements in such reactions.

This example is not typical of the processing methods used generally for particle identification. More generally, a pseudoparameter, which has a unique value for each type of isotope, is generated by suitable manipulations of ΔE and E signals. If this can be accomplished, then events corresponding to production of one type of isotope can be selected for study by merely gating on the pseudoparameter output. For example, in the particle identifier spectra of Fig. 3 a pseudoparameter has been derived whose value (channel number) is dependent only on the type of isotope. Reactions involving the production of ^{11}C can be studied by using a single channel analyzer to select only events in the ^{11}C peak of Fig. 3.

The algorithms used to manipulate the ΔE and E signals and to generate an identification output are based on the Bethe-Bloch equation. For our purpose, this equation can be simplified by the assumption that we are dealing with non-relativistic ions. We then have:

$$-dE/dx = A(Z_e^2/v^2)\ln(2mv^2/I) \qquad (1)$$

where:

dE/dx is the energy loss rate as a function of distance in the track of an ion.

A is a parameter whose value depends on the absorber but not on the ion parameters.

v is the ion velocity.

m is the mass of an electron.

I is the mean ionization potential for absorber atoms ($\approx 12\ Z_A$ eV where Z_A is the atomic number of the absorber element)

Z_e is the effective charge on the ion expressed in electronic units. (At high velocities and for light ions $Z_e = Z$, the atomic number of the ion.)

A slight rearrangement of the equation produces the following result:

$$-dE/dx = B\left(Z_e^2 M/E\right) \ln(bE/M) \qquad (2)$$

where:

B is a constant independent of the ion parameters.

E is the energy of the ion.

M is its mass.

According to Betz[14]), the average ionic charge Z_e is given approximately by the equation:

$$Z_e = Z\ f(v,Z) \qquad (3)$$

where:

$$f(v,Z) = 1 - 1.032 \exp\left[-v/(v_o Z^{0.69})\right] \qquad (4)$$

A graphical representation of these results, adapted from the work of Northcliffe[15]), is shown in Fig. 10. For light ions (e.g., protons), in the energy range above 1 MeV/amu, the value of f(v,Z) is very close to unity, so the ion is fully stripped and its charge is equal to Z. The logarithmic term in Eqn. 2 varies slowly with energy in this range and, together with the 1/E dependence of the main term in Eqn. 2, this produces the approximately -0.7 slope shown in Fig. 10. For light ions at energies below 1 MeV/amu, the ion is not always fully stripped, which explains the curvature in the curves of Fig. 10 that occurs at low values

of E/M. The same effect is apparent extending to much higher velocities. for heavier ions. At very high velocities (E/M >100 MeV/amu for protons) relativistic effects become important and the relationship of Eqn. 1 must be changed to that of the complete Bethe-Bloch equation.

These relationship, as expressed in Eqns. 1-4 and Fig. 10, form the basis for all identifier algorithms. The simplest type of algorithm employed in identifiers approximates the relationship of Eqn. 1 by neglecting the slowly-varying logarithmic term. Assuming that an energy ΔE ($<<E$) is deposited in a ΔE detector of thickness Δx, and that the ions are fully stripped, we then have:

$$E.\Delta E = \Delta x\ MZ^2 \qquad (5)$$

The value of E in this equation is the average ion energy while passing through the ΔE detector and it can be derived from the ΔE and E detector signals. Therefore, according to this approximation, multiplication of the two signals produces an output proportional to the parameter MZ^2 of the ion. Values of MZ^2 for some (relatively) light ions are shown in Table 1. It is easy to see that MZ^2 is a unique parameter for the very light ions, but values of MZ^2, when modulated by fluctuations, become less distinctive for heavier ions. For example ^{13}B and ^{9}C have almost the same value and many similar problems occur for heavier isotopes. Fortunately, early work dealt mainly with light ions (e.g., H and He) where MZ^2 provides a unique value for an isotope.

Two modifications were quickly made to the basic $\Delta E \cdot E$ multiplier scheme of Eqn. 5. The omission of the logarithmic term in Eqn. 5 and, to some extent, the use of Z rather than Z_{eff}, can partially be compensated by introducing a free parameter E_o to produce $(E + E_o)\Delta E$ in the left hand side of Eqn. 5. E_o is adjusted experimentally for the smallest energy dependence in the identifier output. A further correction is required to allow for the fact that, particularly at low energies, the loss in the ΔE detector can be a substantial fraction of the total ion energy. To accommodate this, another free parameter k is introduced so that the energy applicable to transit through the ΔE detector is $(E + k\Delta E)$. Therefore, the final equation becomes:

$$(E + E_o + k\Delta E)\Delta E = MZ^2\Delta x \qquad (6)$$

Table 1 MZ^2 for Light Ions

Mass Amu	H Z→ 1	He 2	Li 3	Be 4	B 5	C 6	N 7	O 8	F 9	Ne 10
1	1									
2	2									
3	3	12								
4		16								
5										
6		24	54							
7			63	112						
8		32	72	128	200					
9			81	144	225	324				
10				160	250	360				
11				176	275	396				
12				192	300	432	588			
13					325	468	637			
14					350	504	686	896		
15					375	540	735	960		
16						576	784	1024	1296	
17						612	833	1088	1277	1700
18						648	882	1152	1458	1800
19							931	1216	1539	1900
20							980	1280	1620	2000
21									1701	2100
22									1782	2200
23										2300
24										2400

Experimental adjustments of the parameters k and E_o permits reasonable performance over a limited range of energies and types of particle.

Another identifier algorithm was developed[8]) in an attempt to broaden the range of types and energies of particles that can be analyzed in an experiment. This approach is based on the observation that a power-law relationship applies in range-energy curves such as those in Fig. 5. Accordingly, the range R of a particle can be represented by

$$R = \alpha E^{\beta} \tag{7}$$

where α is a particle-dependent parameter and β has a fairly constant value near 1.7. If an ion deposits energy ΔE in a detector of thickness Δx, than stops in an E detector, it is clear that the range of a particle of energy $E + \Delta E$ is Δx longer than that of a particle of energy E. Therefore, from Eqn. 7:

$$\Delta x/\alpha = (E + \Delta E)^{\beta} - E^{\beta} \tag{8}$$

The particle-dependent parameter α can therefore be derived by suitable manipulation of the signals E and ΔE. This parameter is independent of particle energy as long as Eqn. 7 holds with the value of β fixed. It qualifies as a pseudoparameter that is uniquely characteristic of a particular isotope.

As presented in the last paragraph, the "range" algorithm depends on the purely empirical observation of the power-law nature of range-energy curves. Actually, this observation can easily be shown to be a direct consequence of the -0.7 slope of the light ion curves in Fig. 10. In fact, the parameter α is equal to $1/MZ_e^2$; therefore, the range algorithm yields essentially the same particle-dependent pseudoparameter as does the multiplier algorithm. However, since it is essentially a range algorithm and does not imply knowledge of rate of energy loss, it is not limited to small losses in the ΔE detector. Furthermore, no experimentally-adjusted parameters are required. These advantages make the "range" algorithm a more convenient and broader-range tool than the "multiplier" algorithm.

Many adaptations and modifications have been made to improve the "range" algorithm to suit particular circumstances. Thus, the special

case of very small ΔE losses can best be handled by an expansion of Eqn. 8. Also modifications can be made allowing the value of β to be a slightly energy-sensitive parameter, thereby permitting some correction for the change in the value of Z_e and for the changing slope of the curves of Fig. 10 at low energies. The power of modern computers has also been employed by using range-energy table look-up procedures and the range algorithm to interpolate between stored values. It should be noted however that none of these adaptations can do better than providing a good value for the parameter α, which is approximately equal to $1/MZ_e^2$. The ambiguities observed for this parameter in Table 1 are not avoided. Their importance depends on the fluctations in the measurements of ΔE and E, a subject which will be discussed in the next section. At least one additional parameter, such as time of flight, is required to assist in resolving such ambiguities.

The design of one type of on-line identifier circuit to perform the calculation of Eqn. 8 is shown in Fig. 11. This is based on the use of the logarithmic properties of semiconductor junctions. As shown in Fig. 11A, the power E^β can be calculated by using a logarithmic element to determine $\ln(E)$, then by multiplying the result by the factor β, and finally by using an inverse logarithmic element to determine $\exp[\beta \ln(E)] = E^\beta$. The function generator shown in Fig. 11B performs this operation on a stepped waveform generated by adding suitably time-gated E and ΔE signals. The output consists of a new stepped waveform whose step is equal to $(E + \Delta E)^\beta - E^\beta$. A gated sampler picks off this step to provide an output pulse representative of $(E + \Delta E)^\beta - E^\beta$. As seen in Eqn. 8, this is proportional to the thickness Δx of the ΔE detector divided by the parameter α. Thus, the output is proportional to MZ_e^2.

A more complex version of this type of identifier is shown in Fig. 12. This is used with a 3-detector telescope. This unit performs similarly to that described in the previous paragraph except that a double stepped waveform is produced by first adding ΔE_1 (the signal from the second ΔE detector in the telescope) to E, then adding ΔE_2 (the first detector signal) to the result at a later time. The resulting steps in the output of the function generator are therefore

proportional to $(E + \Delta E_1)^\beta - E^\beta$ and $(E + \Delta E_1 + \Delta E_2)^\beta - (E + \Delta E_1)^\beta$. According to Eqn. 8, the ratio of these two output steps should always be proportional to the ratio of the ΔE detector thicknesses. The identifier checks that this ratio is correct within statistical limits and rejects events not meeting this criteria. This has the effect of removing events where excessive losses occur in a detector due to occasional high-energy collisions, and also removing events where exceptional low losses occur due to channeling. In this way, the background in identifier spectra is reduced and very rare particles can be studied in the presence of large numbers of uninteresting events. Figure 3 compares results obtained using the 3-counter identifier with those using a 2-counter identifer.

These are examples of on-line identifiers. Other electronic techniques can be used to achieve the same result and off-line processing in computers may employ the same basic methods.

Resolving Power of Identifiers

The power of an identifier system to resolve adjacent isotopes is the most important index of its performance. Even if sophisticated algorithms are used to make the identifier output independent of energy and to have a unique median value for a given isotope, it will still exhibit a spread determined by basic electronic and physical processes. This spread inhibits the power of the identifier to resolve neighboring isotopes. As can be seen in Table 1, the fractional separation in MZ^2 values for hydrogen and helium isotopes is large and resolution of these isotopes is rather easy. It is evident from the table that the situation is not so ideal for heavier isotopes. For example ^{13}B is separated from ^{9}C by only about 0.3% in its MZ^2 value, although it is separated by ~8% from the isotopes ^{14}B and ^{12}B. The instrumental spread shown in the peaks of Fig. 3 is typical of good identifier systems. For example, the full width at half maximum for ^{10}B is ~4%. It is evident that this is a major limitation in identifiers. The basic sources of the spread include the following contributions:

a) Electronic noise causes a spread in ΔE and E signals. Fortunately, in the case of heavy ions, which tend to deposit large energies in detectors, electronic noise is not a major limitation.

b) Detector charge production statistics result in a signal spread given by:

$$dE_{FWHM} = 2.35\sqrt{FE_D\varepsilon} \qquad (9)$$

where:

F is the Fano Factor (0.12 for silicon, ~0·2 for gases).

E_D is the energy deposited in the detector (in ev)

ε is the average energy required to produce a charge pair (3.7 ev for silicon, ~25 ev for gases).

For an energy drop of 20 MeV in a silicon detector, Eqn. 9 predicts a spread of 0.03% in the detector charge and, since the percentage spread is proportional to $1/\sqrt{E}$, this becomes smaller for higher-energy drops. Using gas ionization detectors increases this spread only by a factor of ~3. Therefore, this source of spread is rather unimportant except when using very thin ΔE detectors for light high-velocity ions.

c) Channeling effects may cause small ΔE signals but the correct orientation of the detector makes these effects neligible.

d) Fluctuations in the charge state of ions passing through the ΔE detector cause fluctuations in the energy deposited. These fluctuations can be a major contributor to the spread in identifier signals particularly when heavy ions are measured.

e) The interactions between ions and electrons in the ΔE detector suffer fluctuations both in their number and in the magnitude of the individual exchanges. In very thin detectors, where the number of interactions is small, fluctuations in the magnitude of the energy exchanges cause large variations in the absorbed energy and, occasional large exchanges cause a high-energy tail on an energy-loss distribution curve. This is the Landau

collision regime where the theories of Landau[16]), Symon[17]) and Vavilov[18]) must be used to calculate the energy loss distribution. This process is dominant in cases where the energy loss in the ΔE detector is very small, as when using a very thin ΔE detector to detect lightly-ionizing particles.

When the ΔE detector thickness is large and many ion-electron interactions occur, the energy loss distribution is dominated by fluctuations in the number of collisions and a Gaussian distribution results. Bohr's theory[19]) allows calculation of the resulting spread. For example, 30 MeV α-particles, losing an average of 3 MeV in a silicon detector, exhibit a FWHM spread of 160 keV (or 5%) in their energy loss. However, the percentage spread decreases as the mass of the ion and the energy loss increase. Consequently, this source of fluctuation becomes small for heavy ions.

f) A major source of spread in the ΔE signal may be variations in the thickness of thin ΔE detectors over the sensitive area. Generally speaking, thin detectors can be fabricated with thickness variations in the submicron range. Therefore, these variations are very serious in detectors in the thickness range below 10 μm.

g) Nuclear collisions near the end of a track in the E detector (when the ion is neutralized) provide an energy loss mechanism which does not contribute to the ionization signal. This loss is subject to statistical processes which cause fluctuations in the E detector signal. It can be shown[20]) that these fluctuations are negligible for light ions but can become very significant for heavy ions that only just penetrate into the E detector.

h) Effects which contribute to the so-called "pulse-height defect" associated with heavy ions may cause fluctuations in the E signal as well as causing the signal to be non-linear. These effects include nuclear collisions (referred to in the previous paragraph) and plasma recombination in dense ionization tracks. The resulting non-linearity in E signals causes an error in the identifier output.

i) Dead layers at the interface between ΔE and E detectors also cause the identifier output to become energy-dependent. Since the losses in these dead layers are worst for heavy ions that only just penetrate the ΔE detector this effect is serious for these cases. The effects of g), h) and i) can all be minimized by accepting only those events where the signal in the E detector exceeds a reasonable threshold value

As can be seen from this summary there will inevitably be fluctuations of a few percent in the identifier output and these fluctuations tend to become larger when very small energy losses occur in the ΔE detector or where very heavy ions are detected. Clearly these effects limit the potential of simple ΔE,E identifier systems and other techniques must be adapted to aid in identification. Fortunately, the time of flight technique described in the next section can easily be added to silicon detector ΔE,E systems since thin silicon detectors can provide the required fast timing signals.

Combined ΔE,E and Time of Flight Systems

A ΔE,E telescope directly provides information on the energy of particles (providing that the pulse-height defect is negligible). If the ΔE and E detectors are separated by an appropriate (and convenient) distance, and if the detectors and associated electronics can realize adequate timing accuracy, the telescope can also measure the velocity of particles. By combining the energy and time of flight measurements the mass of each particle can be derived.

The velocity of a non-relativistic ion is given by:

$$v = 1.4\sqrt{E/M} \text{ cm/ns} \quad (10)$$

where E/M is expressed in MeV/amu.

Therefore, 10 MeV/amu corresponds to about 4.5 cm/ns, or approximately 2 ns flight time over a 10 cm path. Very long paths are inconvenient and any divergence of the beam or small angle scattering in the ΔE detector will cause losses of particles from the E detector. Therefore a flight path in the 10 to 30 cm range is convenient. If we retain a 10 cm flight path for this preliminary discussion and use a timing error of 100 ps, which is close to the best yet achieved, the timing uncertainty is approximately 5% of the 2 ns flight time. It is apparent from Eqn. 10 that this results in a 10% error in determining E/M. More generally, a timing error of Δt(ps) will result in an error ΔM given by:

$$\Delta M/M = 2.8 \times 10^{-3}\sqrt{E/M}\ \Delta t/d \quad (11)$$

where the flight path d(cm) is assumed to be accurately defined. Figure 3 shows this result in graphical form. We see that separation of ^{16}O from ^{17}O ($\Delta M/M = 6\%$) at 6 MeV/amu requires a timing accuracy better than 9 ps/cm. A flight path of 10 cm is therefore just adequate for this case if the timing accuracy is 100 ps.

As is indicated by the values in Table 1, MZ^2 values (which are calculated by the standard ΔE,E particle identifier technique) are fairly well separated for isotopes of the same element, but are often overlapped by isotopes of adjacent elements. Fortunately, substantial mass differences exist between isotopes that are of different elements but with similar values of MZ^2. Therefore, a combination of normal ΔE,E identification (yielding MZ^2) and time of flight (yielding M) can provide unique identification where MZ^2 alone would not. This is illustrated by the two-dimensional presentation of Fig. 14. In this particular figure, a very conservative time spread of ±250 ps is assumed and a 10 cm flight path is chosen. As can be seen from this figure, the two-dimensional presentation clearly separates difficult cases such as ^{9}C from ^{14}B and ^{15}B, while the particle identifier (MZ^2) spectrum alone would be very confused in this region.

The results of a combined ΔE,E particle identifier and a time of flight measurement[21]) over a 10 cm path are shown in Fig. 15. This experiment used a telescope containing a 22 μm silicon ΔE detector and a 112 μm silicon E detector which observed the fragmentation induced in heavy nuclei by very high energy-proton bombardment. The contour plot shows peaks corresponding to the production of a broad range of isotopes, a number of which had never previously been observed. The method has been a major tool in studies of the stability of neutron-rich isotopes. Figure 16 shows practical limits to the ability of the combined time of flight and MZ^2 techniques to resolve isotopes. The limit to resolution is dependent on the total particle energy. The optimum ΔE detector thickness is also indicated in this figure.

Conclusion

The techniques described in this brief paper have been the basis of particle identification in the past 20 years. As can be seen from much of the discussion, serious problems occur when these methods are used to identify isotopes of elements of Z >10; therefore, much of the periodic table is inaccessible to these methods except where only elemental (rather than isotopic) identification is required. As heavier ions become the major interest in nuclear science, magnetic analysis, position-sensitive detectors and multielement ionization chambers are assuming increasing importance as particle-identifier tools. The changes in charge state which may occur during transit of heavy ions through detector and target materials are a major problem whatever identification technique is employed.

References

1) F. S. Goulding and B. G. Harvey, Ann. Rev. Nucl. Sci. 25 (1975) 167.

2) R. G. Stokes, J. A. Northrop, K. Boyer, Rev. Sci. Instr. 29 (1958) 61.

3) M. W. Sachs, C. Chasman, D. A. Bromley, Nucl. Instr. and Meth. 41 (1966) 213.

4) A. M. Poskanzer et al., Phys. Rev. Lett. 17 (1977) 1271.

5) J. Cerny et al., IEEE Trans. Nucl. Sci. NS-13 (1966) 1104.

6) F. S. Goulding, et al., IEEE Trans. Nucl. Sci. NS-13 (1966) 514.

7) D. E. Greiner, Nucl. Instr. and Meth. 103 (1972) 308.

8) F. S. Goulding et al., Nucl. Instr. and Meth. 31 (1964) 1.

9) J. Walton et al., to be published in IEEE Trans. Nucl. Sci. NS-25 (1978).

10) R. Eisberg et al., Nucl. Instr. and Meth. 146 (1977) 487.

11) J. P. Ponpon, P. Siffert, Nucl. Instr. and Meth. 112 (1973) 465.

12) M. M. Fowler, R. C. Jared, Nucl. Instr. and Meth. 124 (1975) 341.

13) P. Glassel, R. C. Jared, L. G. Moretto, Nucl. Instr. and Meth. 142 (1977) 569.

14) H. D. Betz, Rev. Mod. Phys. 44 (1972) 466.

15) L. C. Northcliffe, Nucl. Data Tables A7 (1970) 233.

16) W. Landau, J. Phys. USSR 8 (1944) 201.

17) K. Symon, Harvard Thesis (1958), also see High Energy Particles Prentice Hall (1952).

18) P. V. Vavilov, Zh.E.T.P. 32 (1957) 920 transl. J.E.T.P. 5 (1957) 749.

19) N. Bohr, Phil. Mag. 30 (1915) 581.

20) J. Linhard and V. Nielsen, Phys. Lett. 2 (1962) 209.

21) G. W. Butler, A. M. Poskanzer, D. A. Landis, Nucl. Instr. and Meth. 89 (1970) 189.

Figures

1. Block diagram of a 2-detector ΔE,E identifier system.
2. Block diagram of a 3-detector identifier system with a reject channel.
3. Comparative identifier spectra for 2-detector and 3-detector identifier systems.
4. Identifier spectrum for the reaction of 80 MeV α-particles incident on ^{26}Mg target. Note the small number of ^{8}He events.
5. Range-energy curves for hydrogen and helium ions in silicon.
6. Range-energy curves for representative heavy ions in silicon.
7. Cross-sectional view of a gas ΔE, silicon E detector telescope.
8. Electric potential distribution for the gas detector shown in Fig. 7.
9. Map of ΔE,E signals produced by the telescope of Fig. 7 when bombarding a copper target with 288 MeV argon ions.
10. Stopping power in aluminum for various ions (adapted from Ref. 15). The slope lines shown at the top of the figure represent various power laws.
11. Block diagram of a particle identifier using the range algorithm and a 2-detector telescope.
12. Block diagram of a particle identifier for a 3-detector telescope.
13. Spread in mass determination resulting from an uncertainty in a time of flight measurement.
14. Two-dimensional diagram showing mass number (by time of flight) versus particle identifier output ($\propto MZ^2$). Typical spreads are shown on the PI axis and ±250 ps is used as the timing accuracy for a 10 cm flight path.
15. Contour plot of the results of bombarding a heavy nucleus with very high energy protons. The MZ^2 (particle identifier) v mass (time of flight) presentation clearly separates isotopes that would not be resolved in a single parameter measurement.
16. Practical limits to the ability of combined ΔE,E time of flight and MZ^2 identification to resolve isotopes.

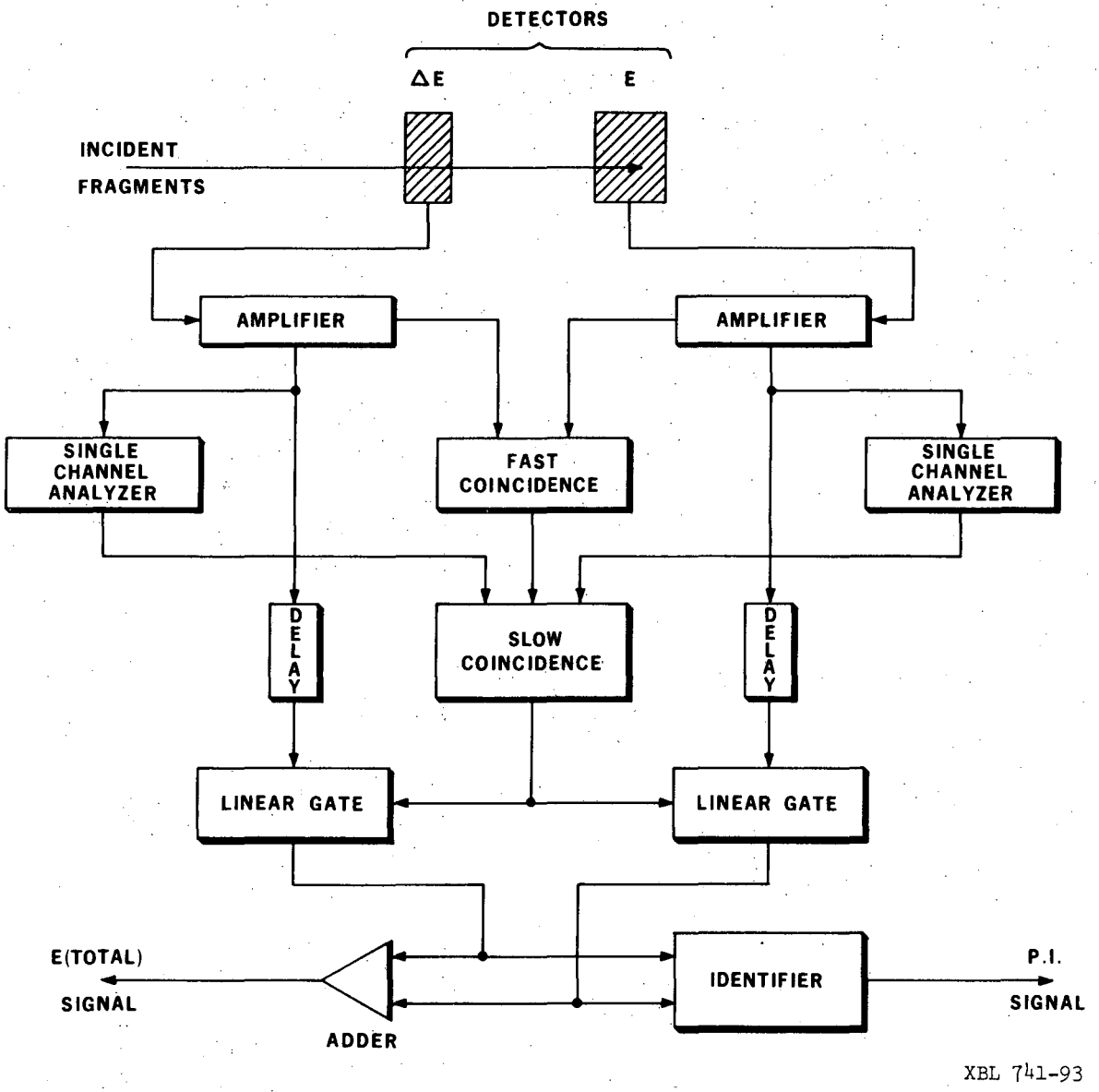
DETECTORS
ΔE
E
INCIDENT
FRAGMENTS
AMPLIFIER
AMPLIFIER
SINGLE CHANNEL ANALYZER
FAST COINCIDENCE
SINGLE CHANNEL ANALYZER
DELAY
SLOW COINCIDENCE
DELAY
LINEAR GATE
LINEAR GATE
E(TOTAL)
SIGNAL
ADDER
IDENTIFIER
P.I.
SIGNAL
XBL 741-93

Figure 1

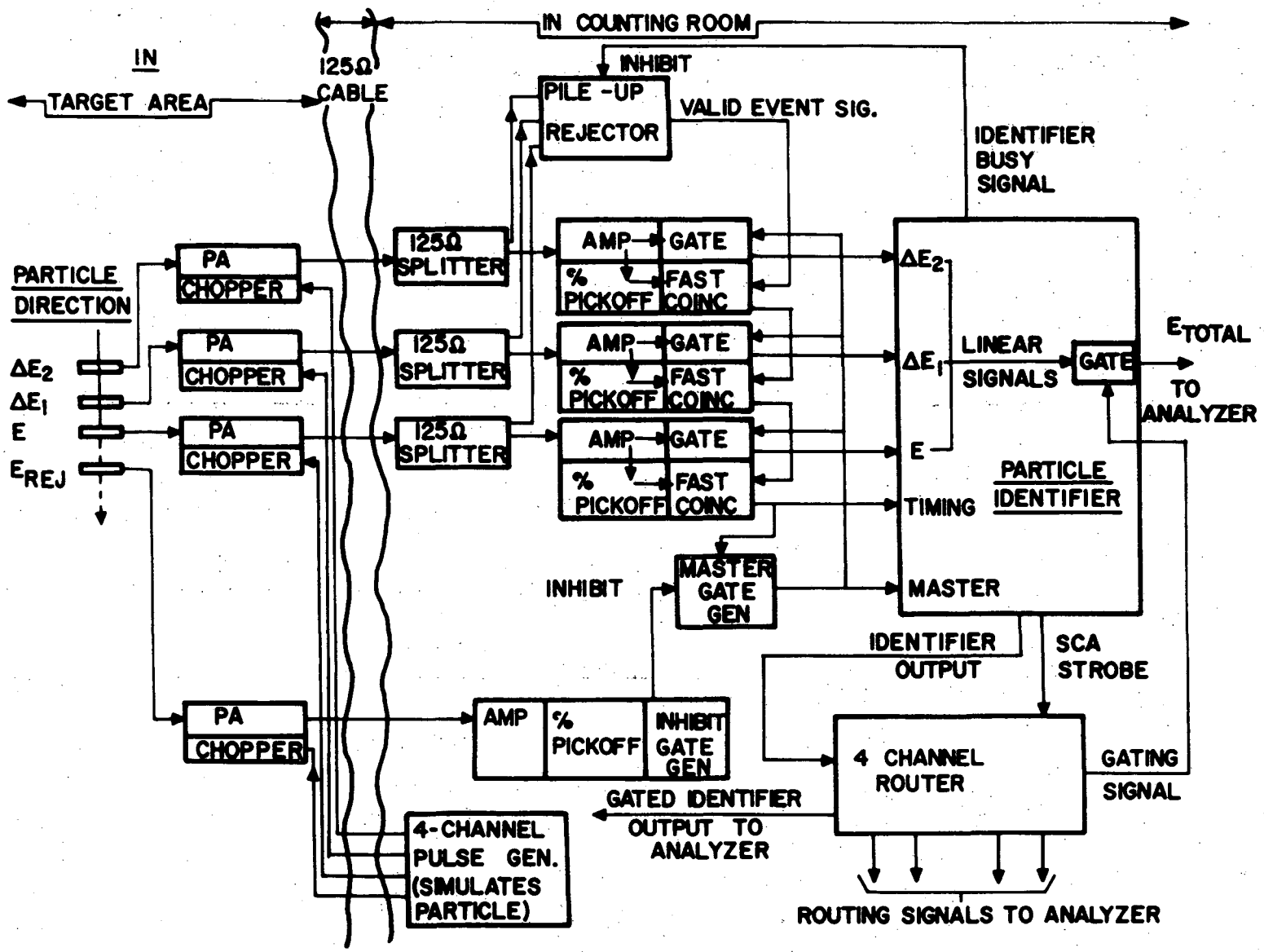

Figure 2

MUB-9659

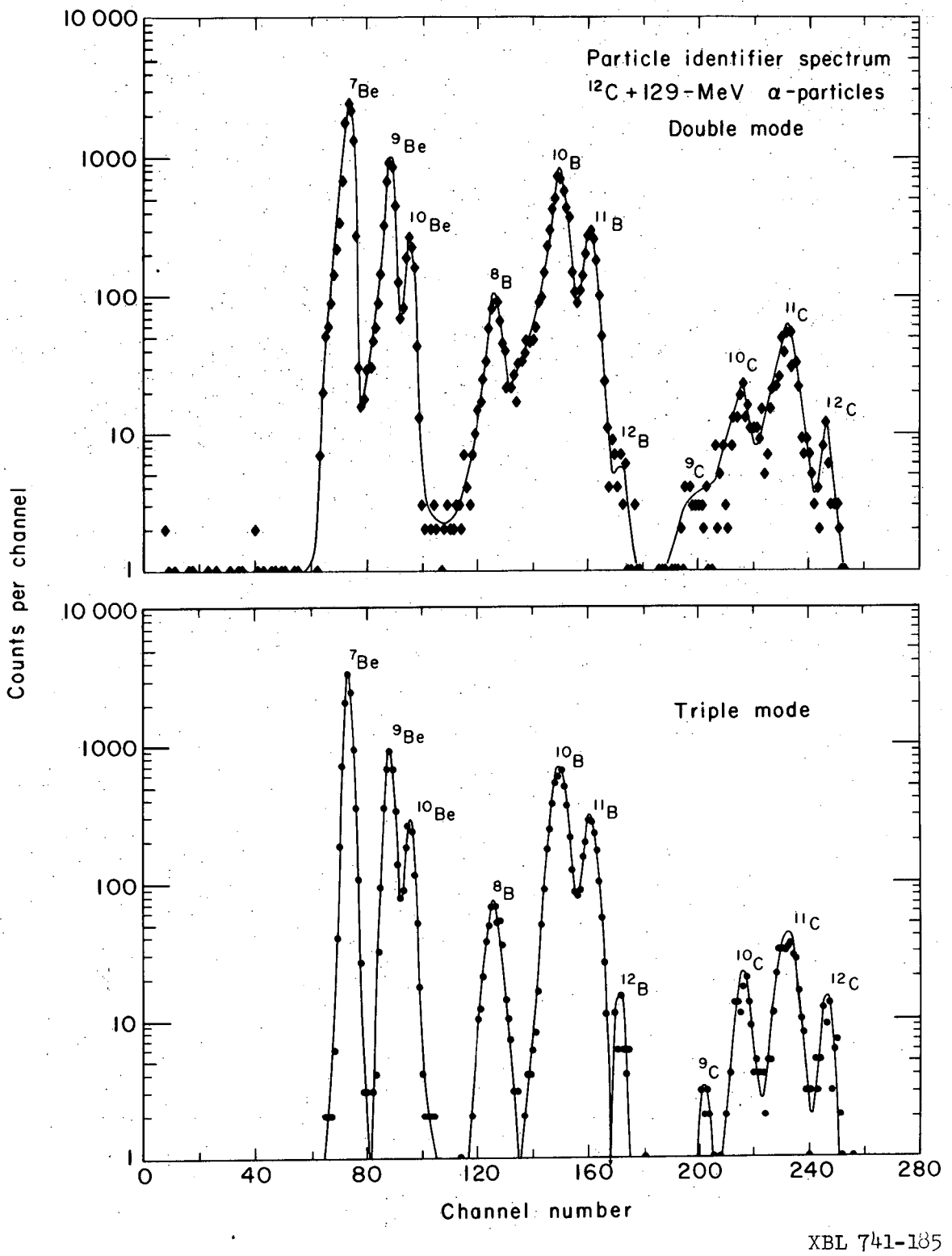
Particle identifier spectrum
^{12}C + 129-MeV α-particles
Double mode
Triple mode
^{7}Be
^{9}Be
^{10}Be
^{8}B
^{10}B
^{11}B
^{12}B
^{9}C
^{10}C
^{11}C
^{12}C
10 000
1000
100
10
1
Counts per channel
0
40
80
120
160
200
240
280
Channel number
XBL 741-185

Figure 3

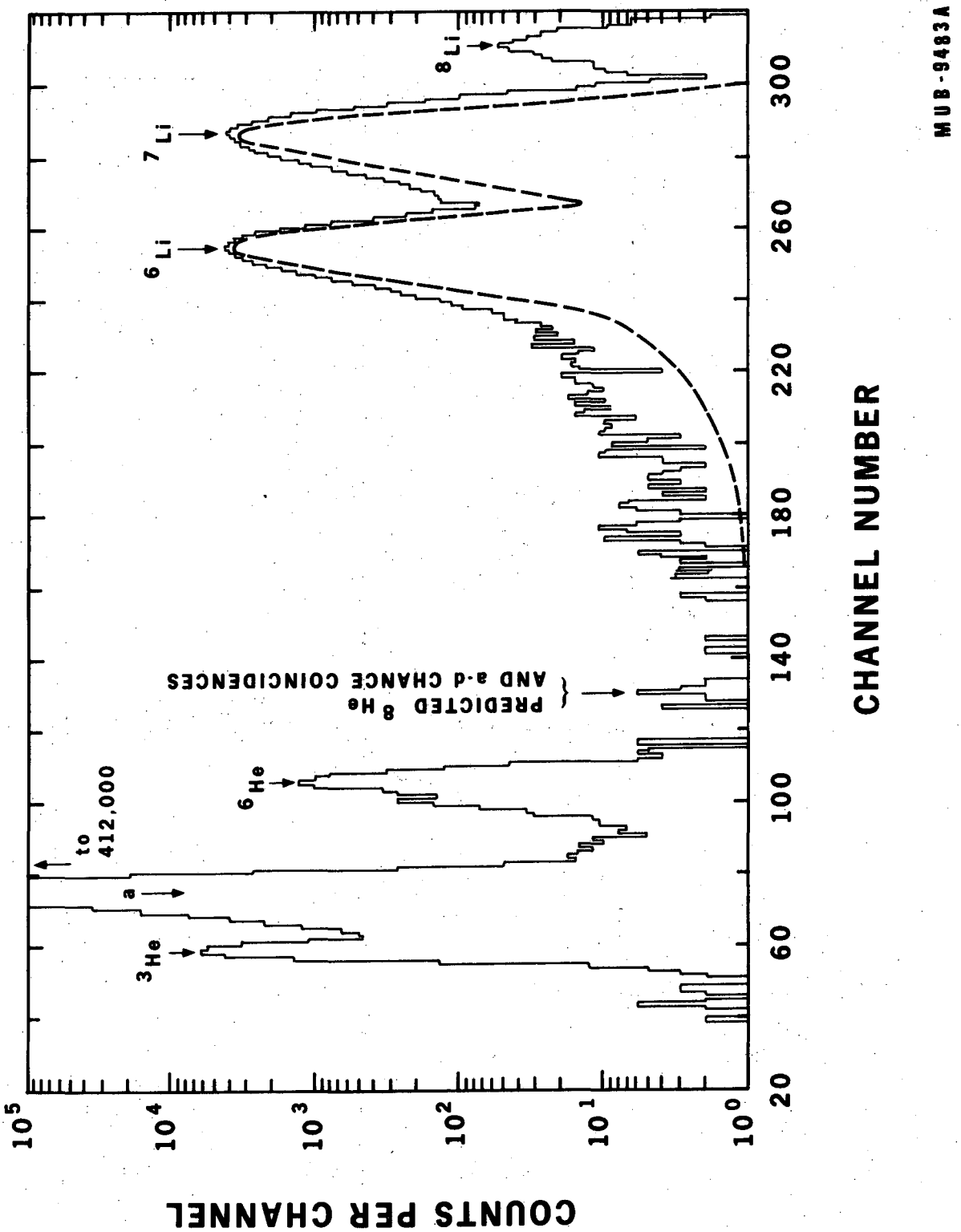
MUB-9483A
CHANNEL NUMBER
COUNTS PER CHANNEL
20
60
100
140
180
220
260
300
10^0
10^1
10^2
10^3
10^4
10^5
^{8}Li
^{7}Li
^{6}Li
PREDICTED ^{8}He
AND a-d CHANCE COINCIDENCES
^{6}He
to 412,000
a
^{3}He

Figure 4

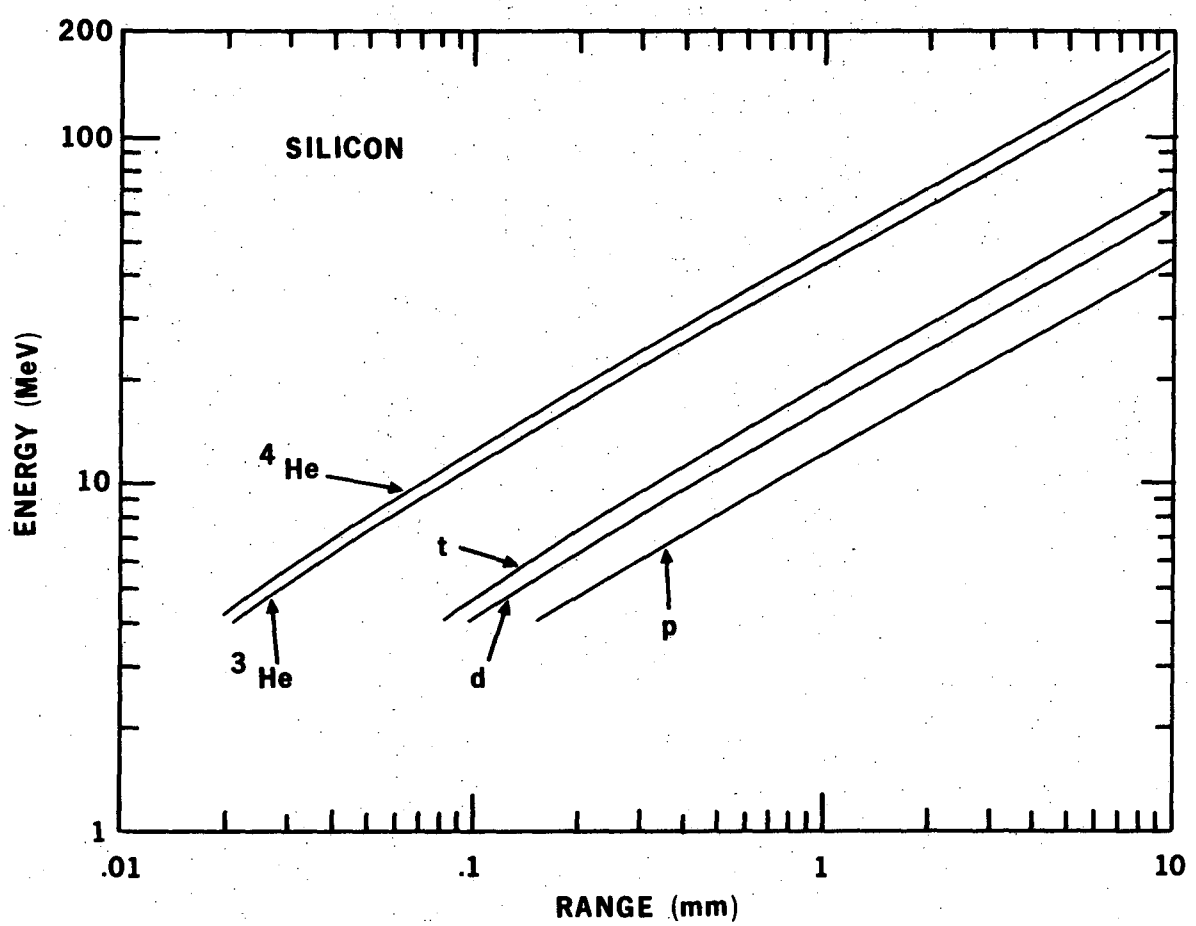

XBL 728-1391

Figure 5

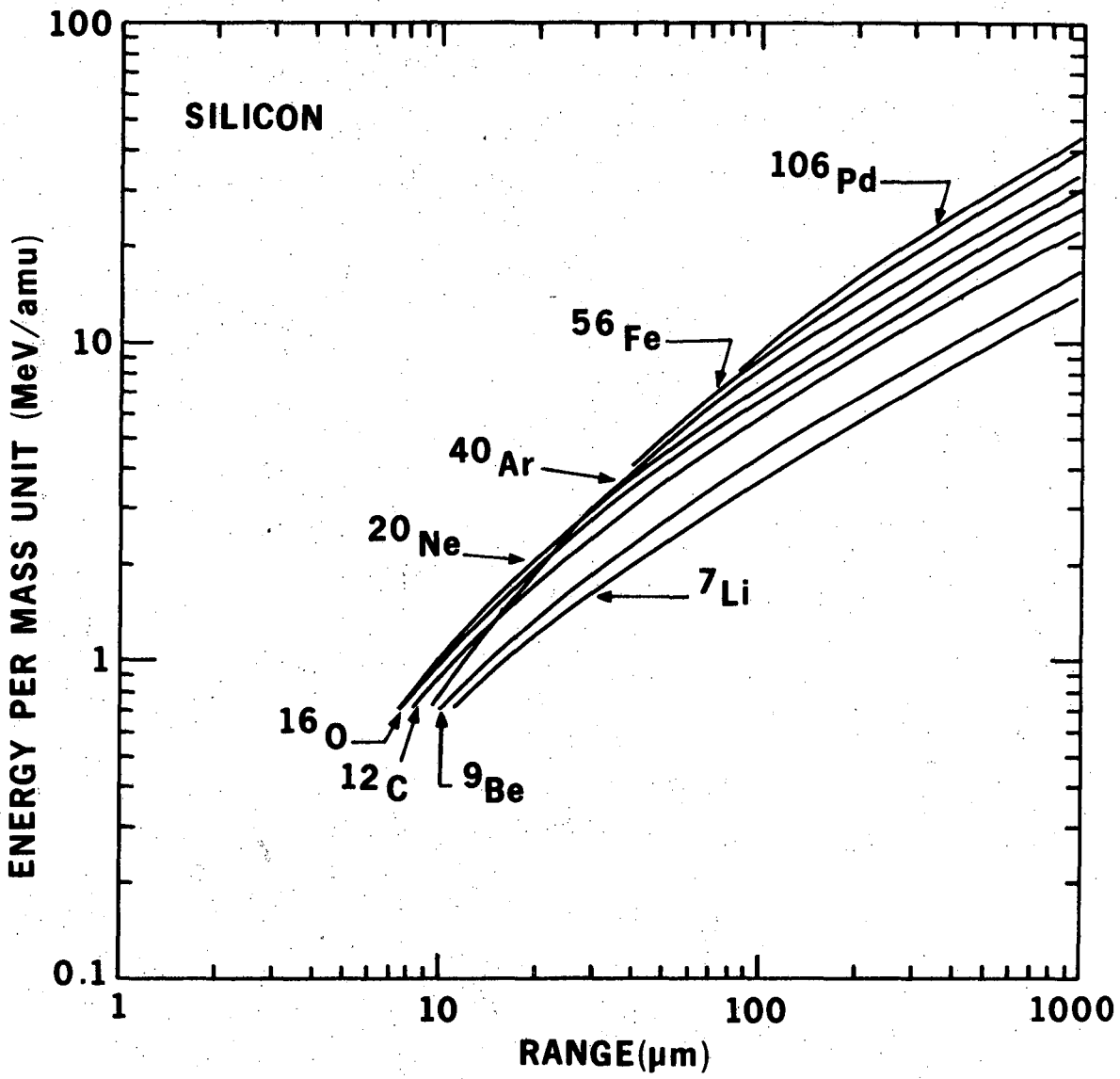
SILICON
ENERGY PER MASS UNIT (MeV/amu)
RANGE(μm)
100
10
1
0.1
1
10
100
1000
106 Pd
56 Fe
40 Ar
20 Ne
7 Li
16 O
12 C
9 Be
XBL 728-1500

Figure 6

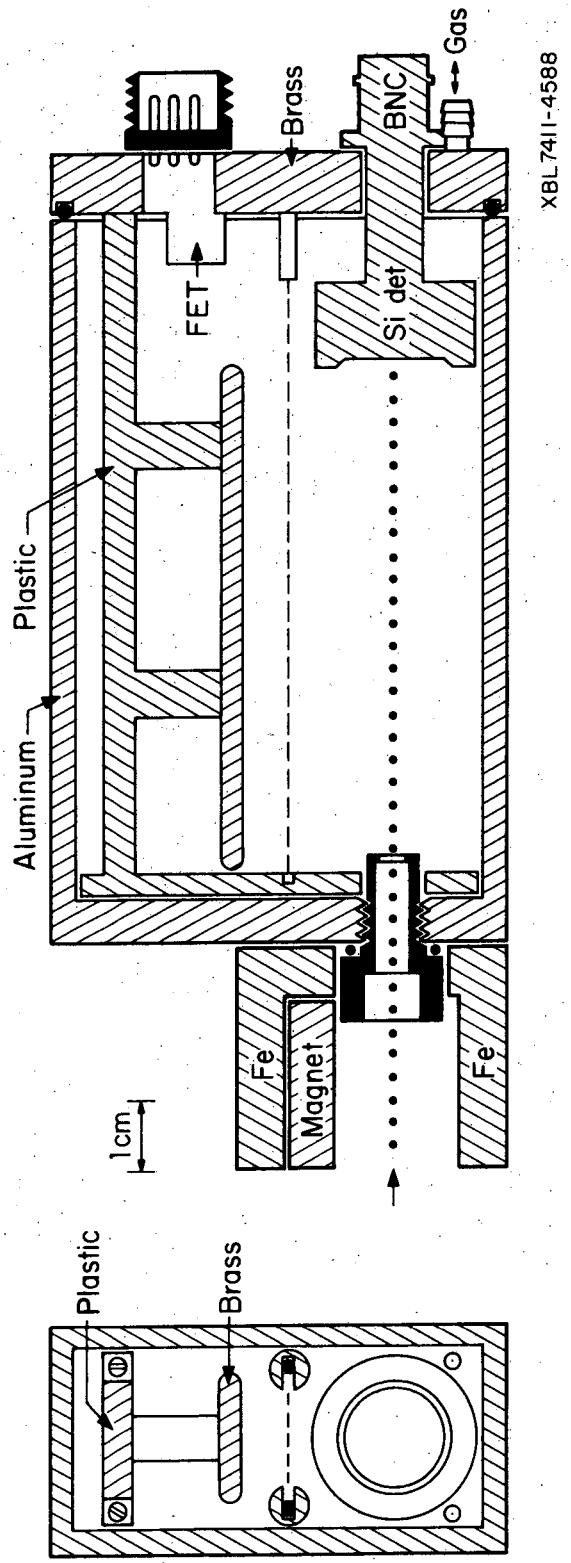
Gas
BNC
Brass
FET
Si det
Plastic
Aluminum
Fe
Magnet
Fe
1cm
Plastic
Brass
XBL 7411-4588

Figure 7

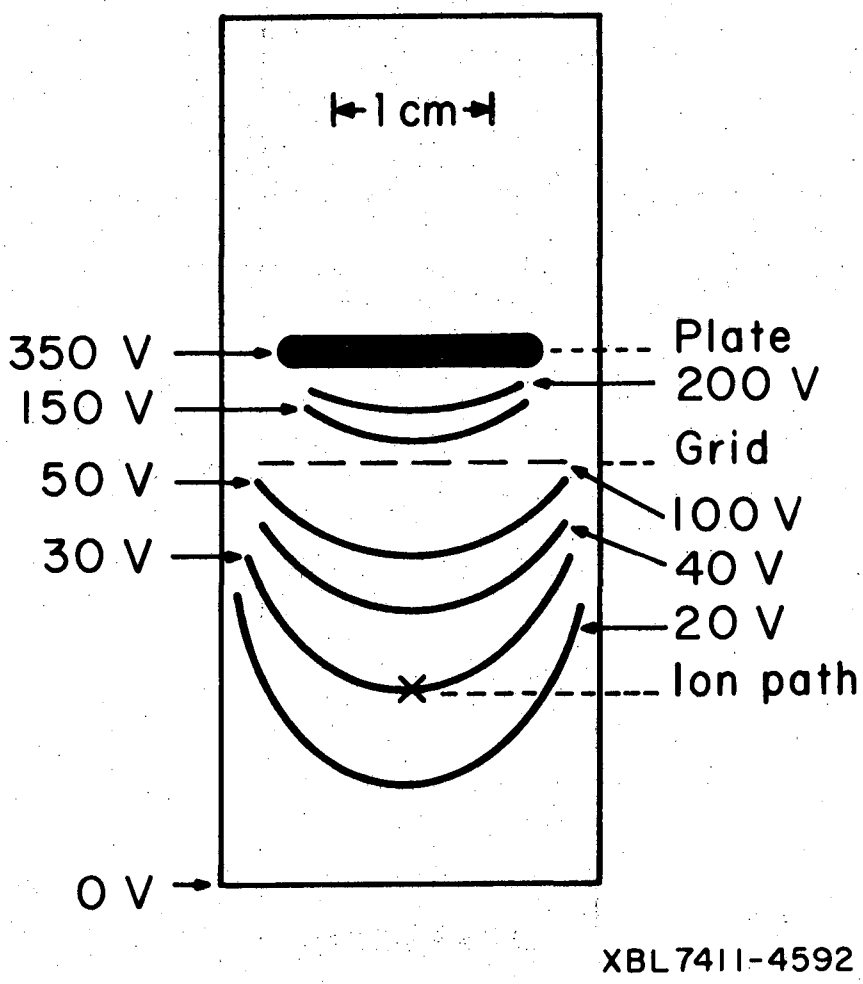
1 cm
350 V
150 V
50 V
30 V
0 V
Plate
200 V
Grid
100 V
40 V
20 V
Ion path
XBL7411-4592

Figure 8

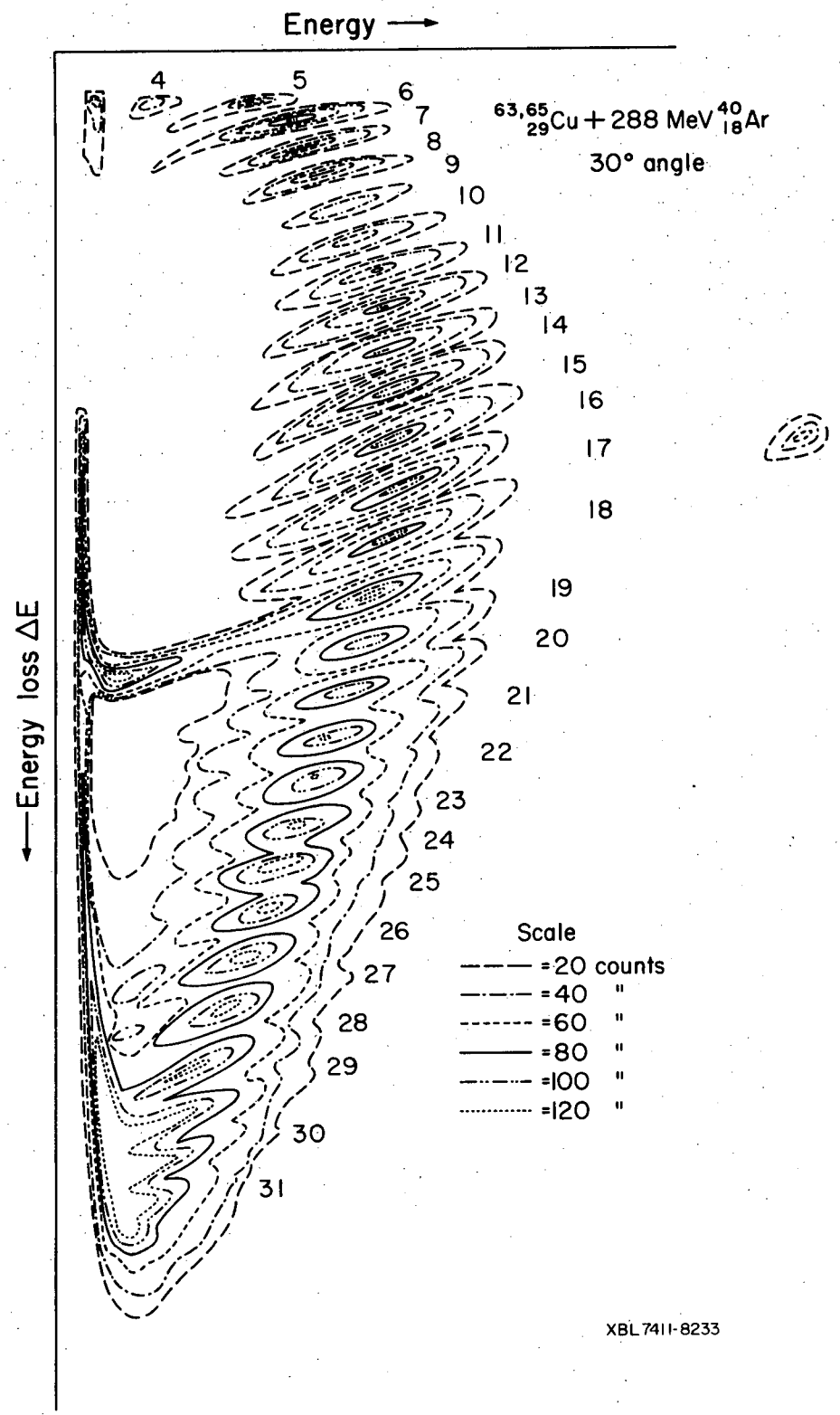
Energy →
←Energy loss ΔE
$^{63,65}_{29}Cu + 288$ MeV $^{40}_{18}Ar$
30° angle
4
5
6
7
8
9
10
11
12
13
14
15
16
17
18
19
20
21
22
23
24
25
26
27
28
29
30
31
Scale
——— =20 counts
—·—·— =40 "
------- =60 "
——— =80 "
—·—·— =100 "
····· =120 "
XBL 7411-8233

Figure 9

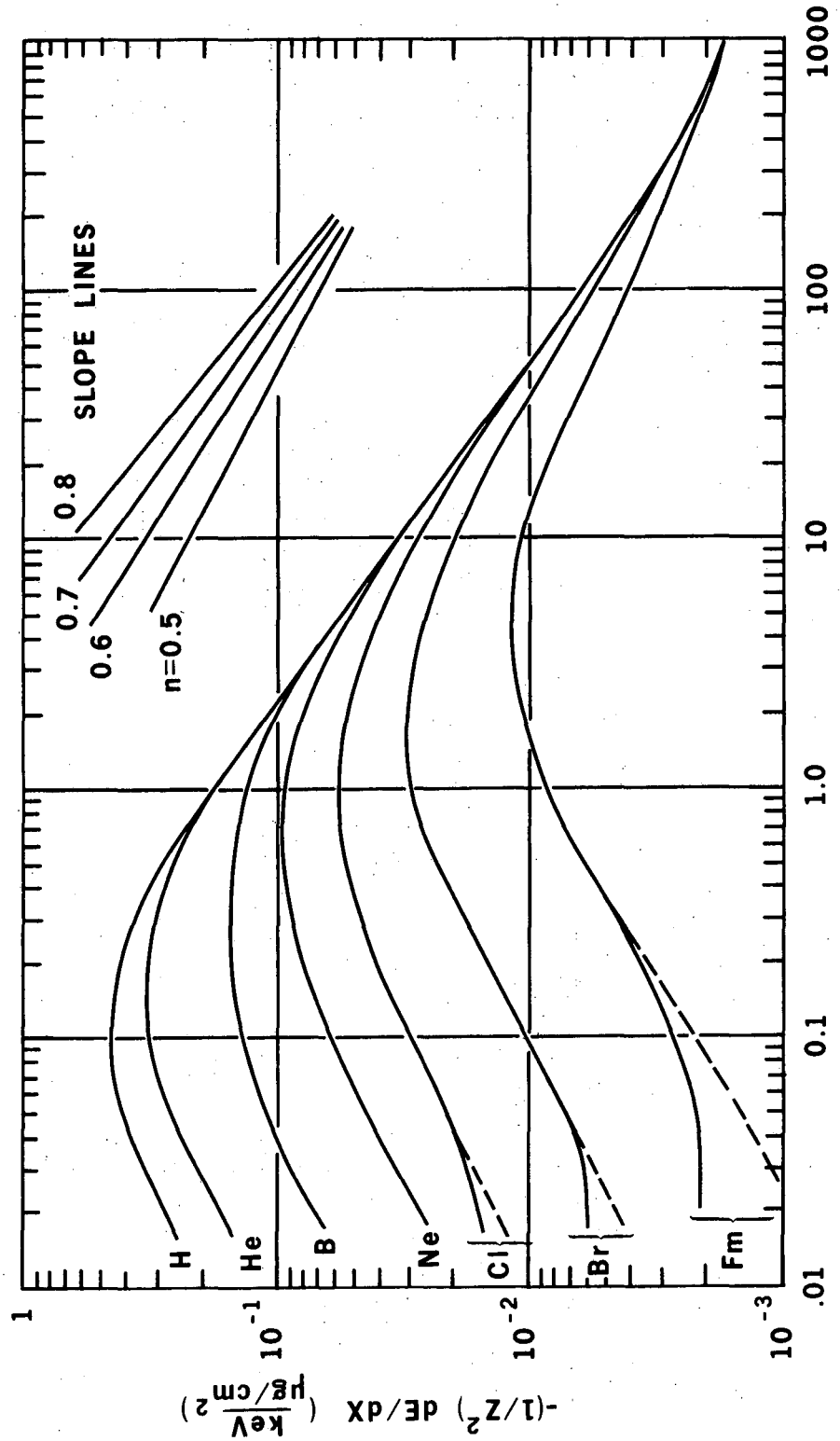

XBL 741-88

Figure 10

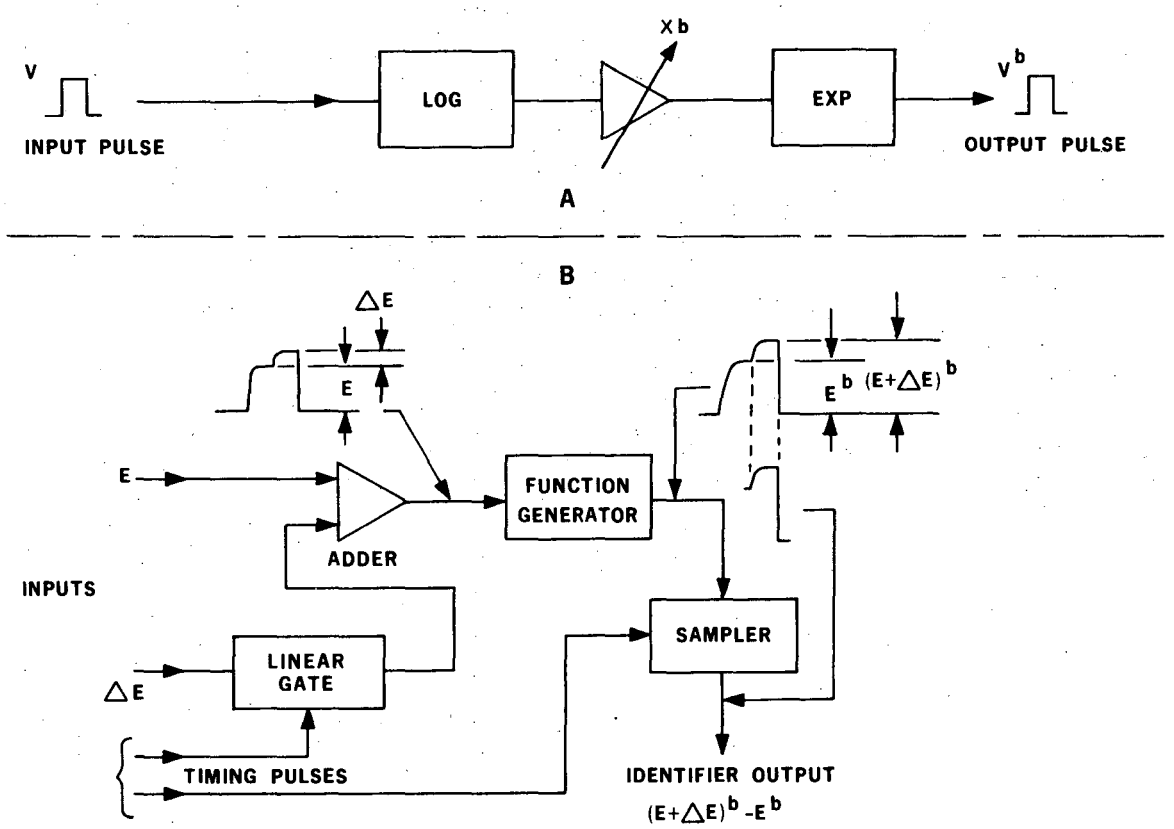
V
INPUT PULSE
LOG
X b
EXP
V b
OUTPUT PULSE
A
B
ΔE
E
E
INPUTS
ADDER
FUNCTION GENERATOR
E b (E+ΔE) b
SAMPLER
ΔE
LINEAR GATE
TIMING PULSES
IDENTIFIER OUTPUT
(E+ΔE) b -E b
XBL 741-92

Figure 11

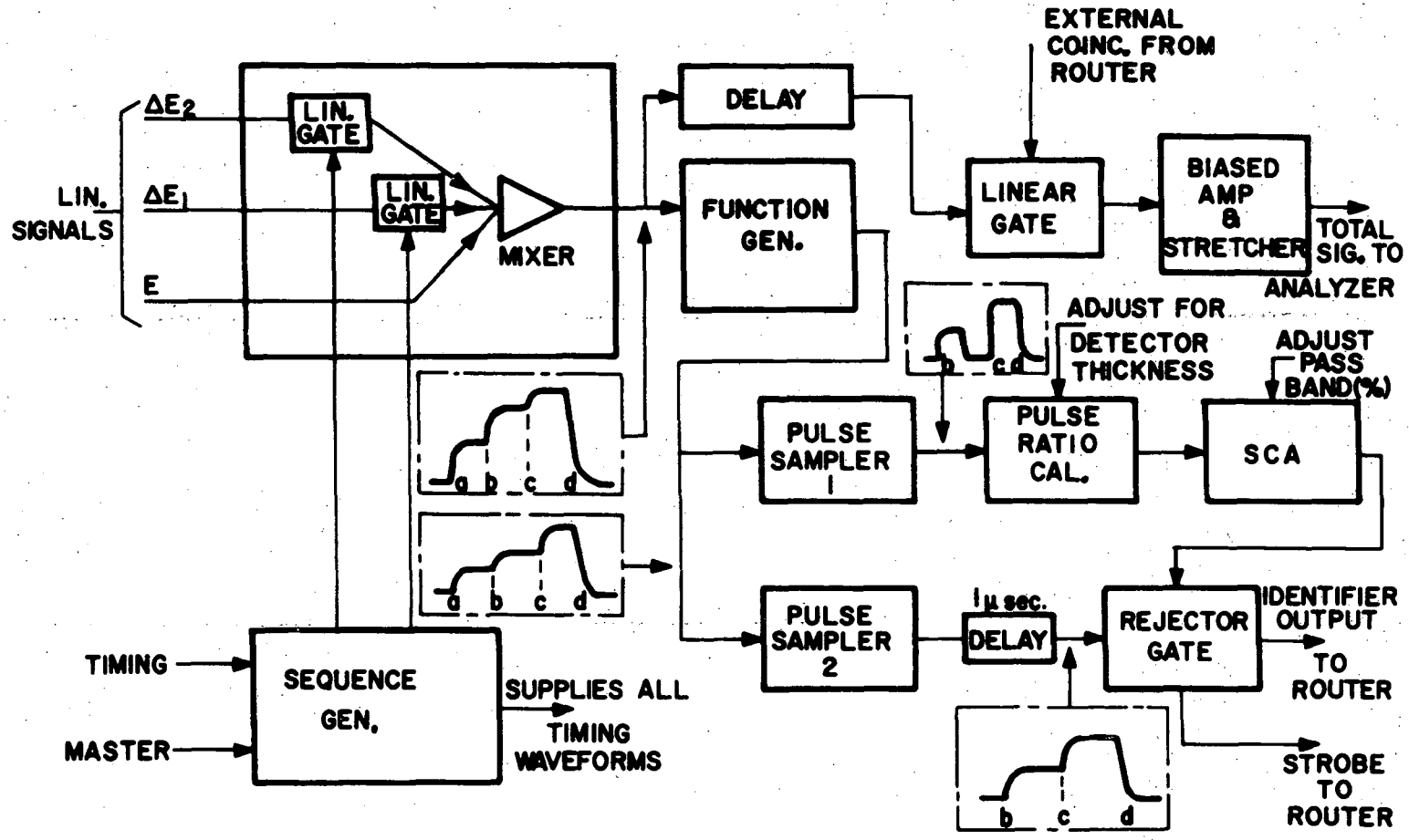

Figure 12

MUB-9660

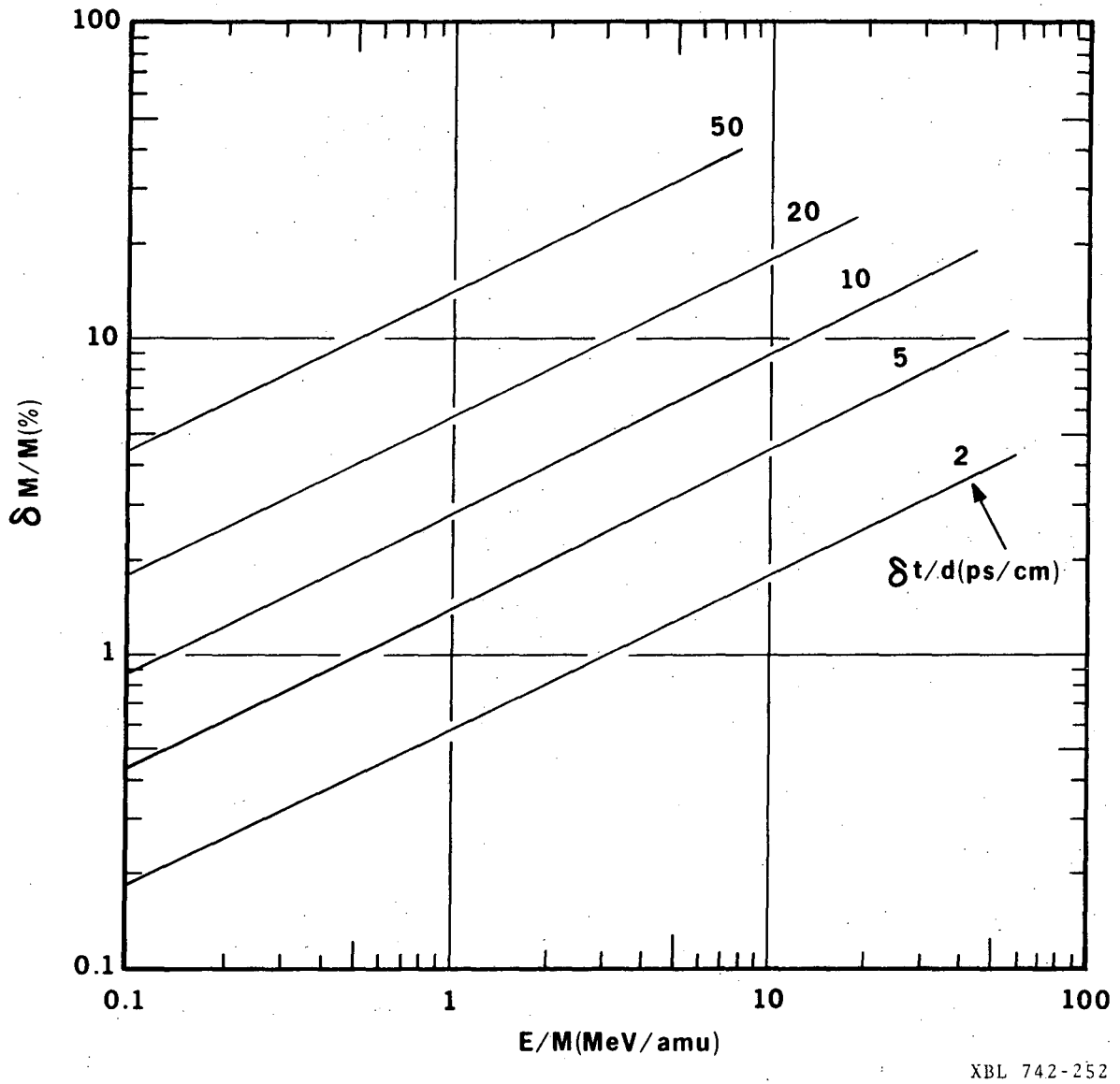
100
10
1
0.1
0.1
1
10
100
δ M/M(%)
E/M(MeV/amu)
50
20
10
5
2
δ t/d(ps/cm)
XBL 742-252

Figure 13

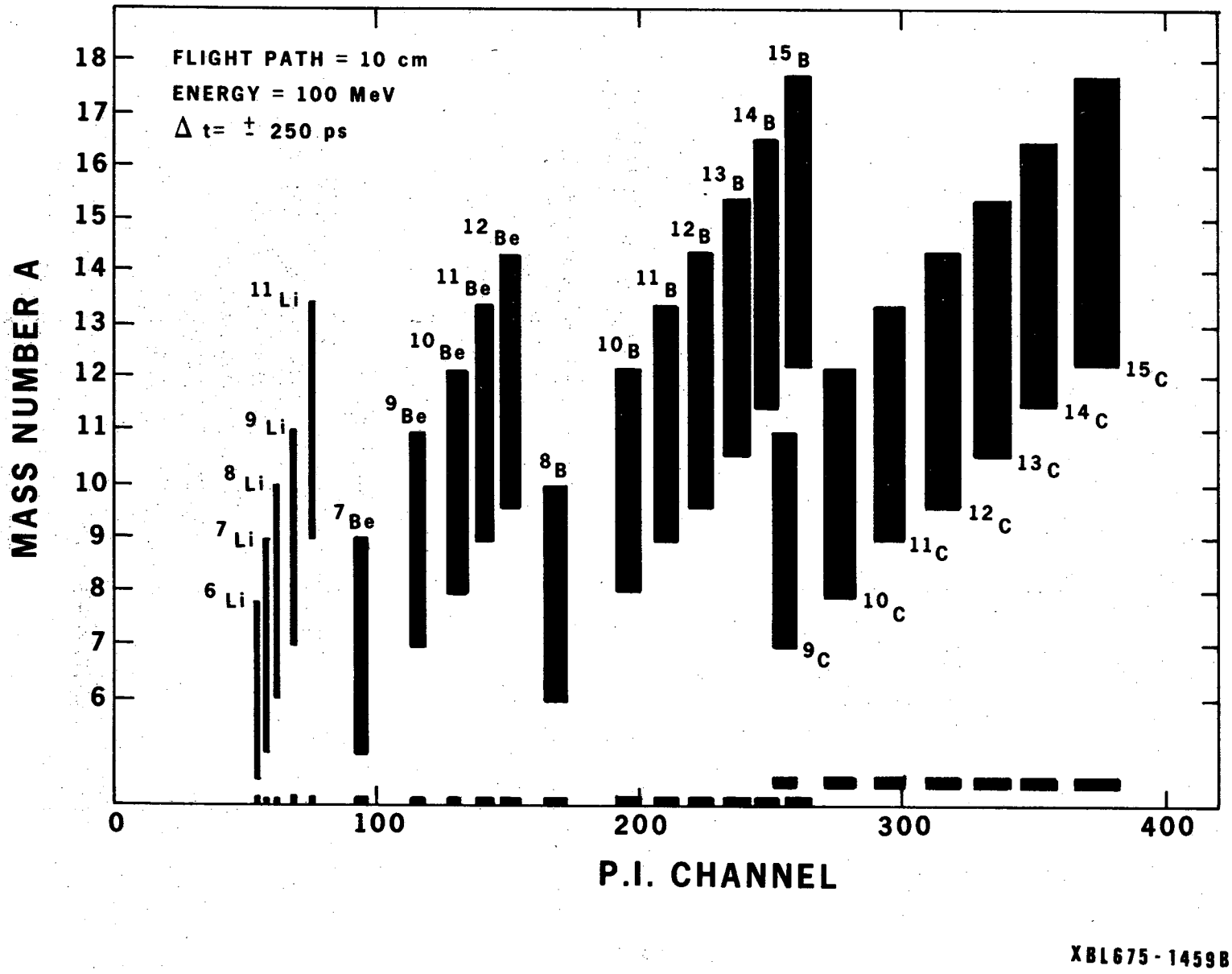

XBL675-1459B

Figure 14

LBL 7995

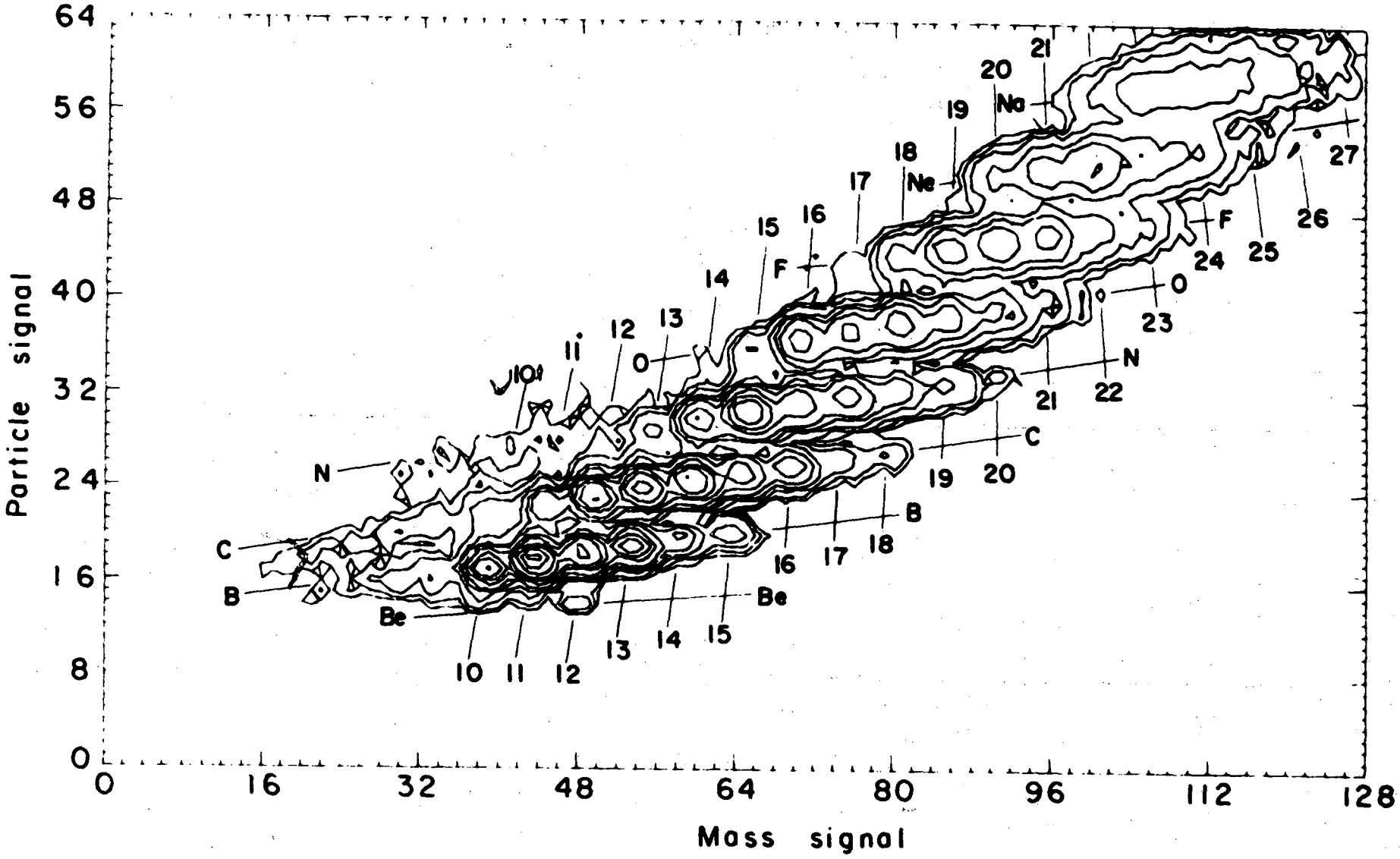

Figure 15

LBL 7995

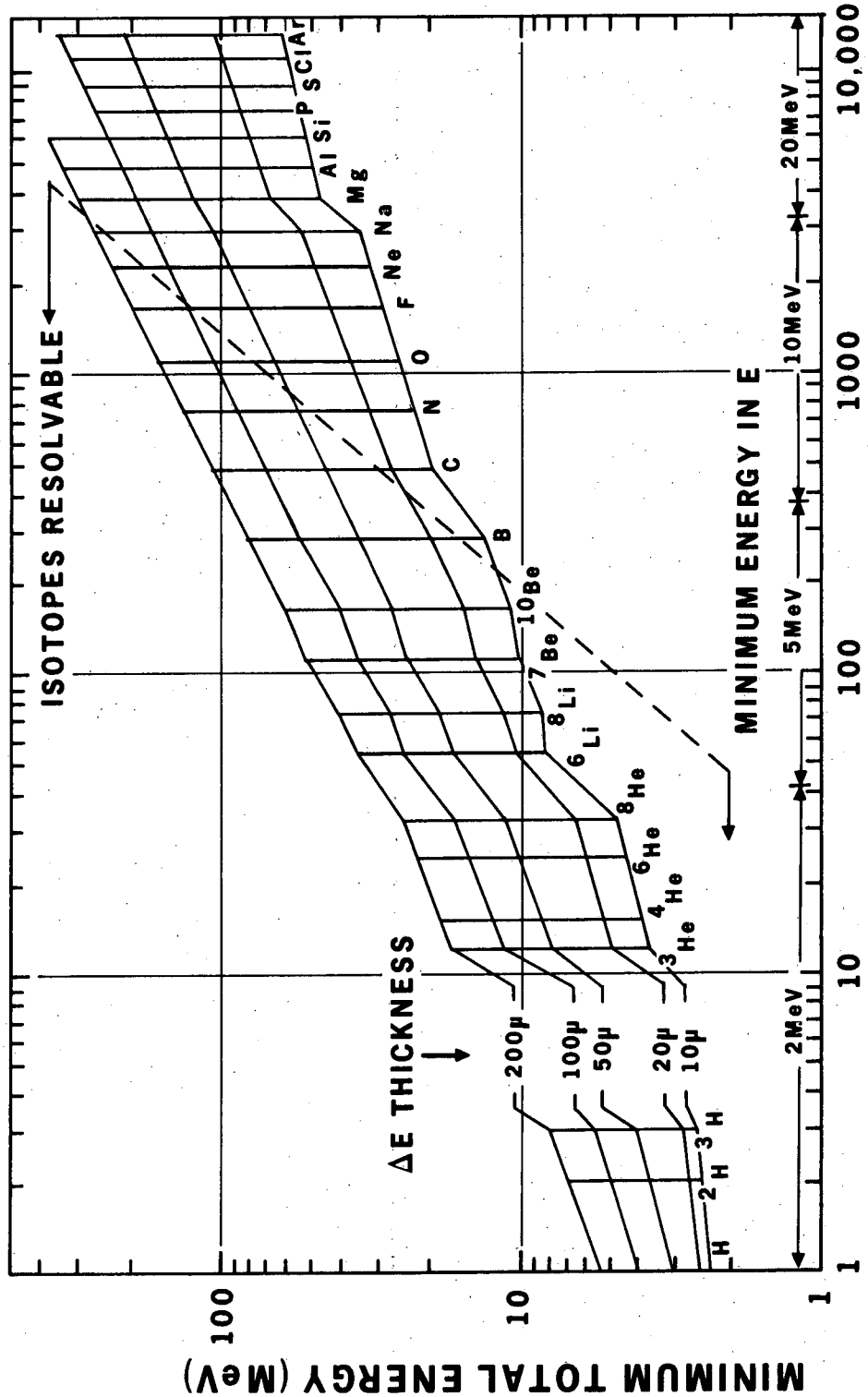
ISOTOPES RESOLVABLE
MINIMUM ENERGY IN E
ΔE THICKNESS
200μ
100μ
50μ
20μ
10μ
2MeV
5MeV
10MeV
20MeV
P S Cl Ar
Al Si
Mg
Ne Na
F
O
N
C
B
10Be
7Be
8Li
6Li
8He
6He
4He
3He
3H
2H
H
1
10
100
1000
10,000
AZ²
MINIMUM TOTAL ENERGY (MeV)
1
10
100
XBL697-3342A

Figure 16

This report was done with support from the Department of Energy. Any conclusions or opinions expressed in this report represent solely those of the author(s) and not necessarily those of The Regents of the University of California, the Lawrence Berkeley Laboratory or the Department of Energy.

TECHNICAL INFORMATION DEPARTMENT
LAWRENCE BERKELEY LABORATORY
UNIVERSITY OF CALIFORNIA
BERKELEY, CALIFORNIA 94720